

# Harmonic (Quantum) Neural Networks

Atiyo Ghosh<sup>1</sup>, Antonio A. Gentile<sup>1</sup>, Mario Dagrada<sup>1</sup>, Chul Lee<sup>2</sup>,  
Seong-hyok Kim<sup>2</sup>, Hyukgeun Cha<sup>2</sup>, Yunjun Choi<sup>2</sup>, Brad Kim<sup>2</sup>,  
Jeong-il Kye<sup>\*, 2</sup>, and Vincent E. Elfving<sup>†, 1</sup>

<sup>1</sup>*PASQAL SAS, 2 av. Augustin Fresnel Palaiseau, 91120, France*

<sup>2</sup>*AI Lab, CTO Div, LG Electronics, 19, Yangjae-daero 11-gil, Seocho-gu, Seoul, 06772, Republic of Korea*

## Abstract

Harmonic functions are abundant in nature, appearing in limiting cases of Maxwell's, Navier-Stokes equations, the heat and the wave equation. Consequently, there are many applications of harmonic functions, spanning applications from industrial process optimisation to robotic path planning and the calculation of first exit times of random walks. Despite their ubiquity and relevance, there have been few attempts to develop effective means of representing harmonic functions in the context of machine learning architectures, either in machine learning on classical computers, or in the nascent field of quantum machine learning. Architectures which impose or encourage an inductive bias towards harmonic functions would facilitate data-driven modelling and the solution of inverse problems in a range of applications. For classical neural networks, it has already been established how leveraging inductive biases can in general lead to improved performance of learning algorithms. The introduction of such inductive biases within a quantum machine learning setting is instead still in its nascent stages, making it a particularly compelling direction for investigation. In this work, we derive exactly-harmonic (conventional- and quantum-) neural networks in two dimensions for simply-connected domains by leveraging the characteristics of holomorphic complex functions. We then demonstrate how these can be approximately extended to multiply-connected two-dimensional domains using techniques inspired by domain decomposition in physics-informed neural networks. We further provide architectures and training protocols to effectively impose approximately harmonic constraints in three dimensions and higher, and as a corollary we report divergence-free network architectures in arbitrary dimensions. Our approaches are demonstrated with applications to heat transfer, electrostatics and robot navigation, with comparisons to physics-informed neural networks included.

---

\*Current: pinostory.com, 1-905, IT Castle, Seoul 08506, Republic of Korea

†email: vincent.elfving@pasqal.com

# 1 Introduction

Harmonic functions can be defined as the solutions to Laplace’s equation  $\nabla^2\phi = 0$ , though there are alternative mathematically-equivalent definitions. Such functions are ubiquitous in nature, appearing in limiting cases of Maxwell’s equations, the heat (or diffusion) equation, the wave equation, irrotational flow in fluid dynamics and first-hitting times of Brownian motion. Consequently, harmonic functions are relevant in many practical settings, including navigation in robots [1], electrostatic imaging [2], heat transport [3], to name but a few examples. Finite elements methods (FEM) often represent the state-of-art approach in solving the corresponding equations, with attempts specifically targeting harmonic functions [4]. In contrast to FEM, machine learning based approaches offer the chance to assist with data-driven modelling (analogous to [5]), handle noisy-data/boundary conditions, solve inverse problems for design optimization [6], perform transfer learning and model discovery [7]. In this particular case, effective learnable and differentiable representations of harmonic functions could therefore be key in multiple fields. However, there have been few attempts dedicated at constructing harmonic functions in either quantum or conventional machine learning: we hereby intend to address this point.

**Variational Quantum Algorithms** Quantum computing is a computational paradigm that holds theoretical promise for exponential speedups over conventional computers in, for example, factoring prime numbers [8] and solving linear systems of equations [9]. However, the practical application of such provably advantageous algorithms is hindered by the lack of fault-tolerant quantum computers, which are still thought to be years away in terms of development. In spite of such theoretically-guaranteed computational advantages being limited to future devices, there have already been indications of experimental quantum advantage having been achieved for certain restricted classes of problems [10, 11]. While such experimental advantages have been demonstrated, it remains to find advantages in applications which have wider practical application. A promising avenue for achieving practically-relevant quantum advantage within currently available and near-term noisy intermediate-scale quantum (NISQ) computers consists of variational quantum algorithms [12]. There are several parallels between variational quantum models and neural networks (NNs). For example, both can be seen as parameterised functions which are optimised with a conventional optimiser, achieving universal approximation properties [13, 14]. Furthermore, there are means of achieving automatic differentiation directly on quantum circuits [15, 16], which has been used in quantum algorithms for classification and regression tasks [17], solving differential equations [18, 19], model discovery [20] and extremal learning [21].

Quantum NNs hold the promise of being advantageous in terms of the *expressivity* [22, 23], offered by parameterised quantum circuits, while the *trainability* of variational quantum algorithms is a vital aspect of reaching practical quantum advantage [24]. In fact, many quantum circuits are susceptible to trainability issues [25, 26], e.g. large regions of parameter space exhibit exponentially-vanishing

parameter gradients with respect to loss functions, so called ‘barren plateaus’.

One successful means to mitigate barren plateaus has been to include inductive biases within quantum circuit designs [27, 28]. It has even been argued that, in some settings, including inductive biases in quantum circuits is a prerequisite for quantum advantage [29]. Including inductive biases in conventional NNs has been a staple of progress in machine learning, e.g. ranging from convolutional neural networks [30] and geometrically-invariant networks [31] through to recent examples such as Hamiltonian neural networks [32] and physics-informed neural networks [5]. However, the use of inductive biases in designing quantum circuits and quantum machine learning models is still a nascent field, though there is a growing research interest on this front [33, 34].

**Physical Inductive Biases in Conventional Machine Learning** Of particular relevance to our work on harmonic functions are physics-informed neural networks (PINNs) [5], which use derivatives of NNs with respect to their inputs as a regularisation term to provide an inductive bias towards a given differential equation, including potentially towards harmonic functions. Even though this concept was introduced decades ago [35], PINNs have only recently garnered much attention. Despite their popularity, the difficulty of training PINNs has been well-documented [36, 37]. Strategies to try and mitigate these difficulties have included domain-decomposition [38], online-adaptivity of loss functions to facilitate training [39], curriculum training [36] and constraining network architectures to satisfy given boundary conditions [6, 40]. For a wider overview of PINNs, we direct the interested reader to a recent review [41].

Related to PINNs, there has been a growing recent interest in applying machine learning towards differential equation problems, such as the solution of families of differential equations [42, 43], or facilitating the solution via dimensionality reduction [44]. Finding NNs which directly obey a given (linear) differential operator as a hard-constraint has attracted some recent attention [45]. In particular, however, constructing divergence-free networks was only recently extended to dimensions other than three, during the preparation of this work [46]. In addition to physical inductive biases encodable via differentiable equations, there have also been recently developed methods to effectively impose energy-conservation on learnt representations [32, 47].

**Inductive Biases in Variational Quantum Algorithms** In the context of variational quantum algorithms, inductive biases are often referred to as problem-inspired ansätze. A well-established example is the unitary coupled cluster ansatz for modelling the ground-state energy of molecular Hamiltonians [48]. Hard-constraints in ansätze for combinatorial optimization have also been previously reported [49]. Analogously to how neural architecture search [50] might learn architectures with given inductive biases, there have been developments on adaptively constructing ansätze for molecular simulations [51]. Another well-known paradigm concerning the adoption of inductive biases in the context of variational quantum algorithms refers to the characterisation of quantum

systems. In this case, learning a full dynamic map describing a quantum process (i.e. performing ab initio a quantum tomography) is unfeasible already for systems of very few qubits [52]. However, the system dynamics can be modelled constraining such maps by knowledge of (parametrised) generators of the dynamics (e.g. the system’s Hamiltonian [53]) and of their eigenstates [54]. Similarly to aforementioned ansätze in molecular simulations, such parametrised generators can also be made adaptive [55].

A promising candidate quantum algorithm to combine with harmonic function inductive biases are the Differentiable Quantum Circuits (DQC), outlined in [18]. The latter uses an advantageous latent space representation for the mapping of input data, and derivatives of quantum circuits with respect to their inputs to solve given (also non-linear) differential equations. Equipped with appropriate loss functions taking into account soft-constraints, as well as automatic differentiation rules providing an effective surrogate of backpropagation rules in conventional NNs, such architectures can then be regarded as a quantum PINN. For simplicity we refer to such differentiable quantum circuits as qPINNs, but we emphasise that this terminology is not widely used. Training qPINNs poses in principle no less issues than PINNs of equivalent expressivity, and this limitation might be exacerbated by the sheer number of parameters that can potentially describe vast quantum circuits, which can complicate training [25, 26]. Such considerations emphasise the need for relevant inductive biases in quantum circuits.

Our main focus in this work is to incorporate inductive biases for harmonic functions in both quantum and conventional machine learning. We demonstrate exactly-harmonic functions in conventional and quantum NNs for simply connected two-dimensional domains using complex-valued NNs. For multiply-connected domains, we provide a domain decomposition methodology which allows us to continue using complex-valued, conventional NNs as harmonic function representations. We demonstrate how using such divergence-free architectures can provide an inductive bias to learn harmonic functions in both quantum and classical NNs. We use example problem settings from heat distribution, electrostatics and robot navigation to demonstrate the effectiveness of our proposed inductive biases in both conventional and (simulated) quantum NNs. We provide implementations of our classical architectures in the supplementary material to facilitate adoption of these inductive biases. We provide methodologies to derive exactly divergence-free architectures for both quantum and conventional NNs in arbitrary dimensions. Previous work [45] had been limited to three dimensions. However, we are now aware during manuscript preparation of recently-published material outlining similar divergence-free architectures as those which we outline [46].

**Note on terminology** We consider both conventional (or classical) neural networks as well as quantum circuits for representations of harmonic functions. To avoid confusion, henceforth we will use the term ‘neural network’ to refer to statements applying to both quantum circuits and conventional neural networks.

When seeking to refer specifically to quantum circuits or conventional NNs, we will explicitly state as such.

## 2 Theory

### 2.1 Exact-Harmonicity: Holomorphic Networks on Simply Connected Domains

We first recount some well-established relationships between real parts of holomorphic functions and harmonic functions (see, e.g. [56] for an accessible introduction/refresher to these topics).

Denote by  $Y^X$ , the set of all functions from a set  $X$  to a set  $Y$ . Given a function  $f : \mathbb{C} \rightarrow \mathbb{C}$  defined by  $f(x + iy) = u(x, y) + iv(x, y)$ , with  $x, y \in \mathbb{R}$  and  $u, v \in \mathbb{R}^{\mathbb{R}^2}$  recall that  $f$  is *holomorphic* if the Cauchy-Riemann equations hold:

$$\frac{\partial u}{\partial x} = \frac{\partial v}{\partial y} \quad \text{and} \quad \frac{\partial u}{\partial y} = -\frac{\partial v}{\partial x} \quad (1)$$

Taking the partial derivative of the first equation of 1 with respect to  $x$  and the second equation with respect to  $y$  and summing both equations yields  $\frac{\partial^2 u}{\partial x^2} + \frac{\partial^2 u}{\partial y^2} = 0$ . Therefore  $\Re(f)$  is a harmonic function, where  $\Re$  takes the real part of a complex value.

Consequently, we can derive an exactly-harmonic neural network by constructing a holomorphic neural network.

**Conventional Neural Networks** Construct a complex-valued neural network  $\text{NN}_c : \mathbb{C} \rightarrow \mathbb{C}$  by taking a multi-layer perceptron with complex valued weights in linear layers, and holomorphic activation functions, for example  $\sigma(z) = \sin(z)$  or  $\sigma(z) = \exp(z)$ . Define a function  $c : \mathbb{R}^2 \rightarrow \mathbb{C}$  by  $c(x, y) = x + iy$ . Now we can define a harmonic neural network  $\phi_{CH} : \mathbb{R}^2 \rightarrow \mathbb{R}$  by

$$\phi_{CH} = \Re \circ \text{NN}_c \circ c. \quad (2)$$

The resulting output is a holomorphic function, because the composition of holomorphic functions is itself holomorphic [56], and each constituent layer of  $\text{NN}_c$  being expressed by linear functions, it is also automatically holomorphic.

Finally, we note that there has been much research into complex-valued conventional NNs, but we consider a meaningful review of them to be outside the scope of our work, referring to [57] for an introduction to their theory and application.

**Quantum Neural Networks** We now consider implementing a quantum neural network (QNN) resorting solely upon operations that satisfy holomorphicity, whilst stressing how alternative forms of harmonic QNNs may well be constructed. We start by defining a variational state  $|\Psi_{\theta, x, y}\rangle$ , parametrised by  $\theta$ -dependent unitaries  $\hat{U}_{\theta_k}$  as well as a quantum feature map (QFM) - e.g. of

Chebyshev tower type [18] - used to port the input variables to the Hilbert space acted upon by  $\hat{\mathcal{H}}$ :

$$|\Psi_{\theta,x,y}\rangle = \hat{\mathcal{U}}_{\theta_2} \text{QFM}(x,y) \hat{\mathcal{U}}_{\theta_1} |\emptyset\rangle; \quad \begin{cases} \phi_Q(x,y) = \langle \Psi_{\theta,x,y} | \hat{\mathcal{H}} | \Psi_{\theta,x,y} \rangle & (3a) \\ \phi_{QH}(x,y) = \Re\{\langle \emptyset | \Psi_{\theta,x,y} \rangle\} & (3b) \end{cases}$$

where  $|\emptyset\rangle$  represents a reference state. A QNN is typically modelled as a measurement of a cost Hamiltonian  $\hat{\mathcal{H}}$  (Eq. 3a), but alternatively we propose the modified ‘quantum kernel’ [22, 58] in Eq. 3b. We now show that such kernel setting allows for constructing a function that is harmonic over the inputs  $x$  and  $y$ , while still measurable on a realistic quantum computer. The former can be achieved by introducing a novel type of feature map, of the form  $\text{QFM}(x,y) = e^{-(x+iy)\hat{\mathcal{H}}}$ . For  $x = 0$ , this represents a unitary evolution generated by  $\hat{\mathcal{H}}$ , similar to the Hamiltonian evolution feature maps in [18, 16]. For non-zero  $x$ , the operation is generally non-unitary, rendering it not directly implementable with quantum gates on hardware. However, stemmed from the context of ground-state preparation in quantum simulation, the Quantum Imaginary Time Evolution algorithm was recently developed [59, 60, 61]: using this formalism and generalising to complex numbers including a real part, we can symbolically represent:

$$\phi_{QH}(x,y) = \Re\left\{\sum_m c_m(\theta_1) \langle \emptyset | \hat{\mathcal{U}}_{\theta_2} | \psi_m \rangle e^{-(x+iy)E_m}\right\}. \quad (4)$$

where  $E_m$  is the  $m$ -th (scalar) eigenvalue of Hamiltonian  $\hat{\mathcal{H}}$  and the state  $|\Psi\rangle$  was decomposed into the basis set  $|\psi_m\rangle$  with coefficients  $c_m(\theta_1)$ , summing over all  $2^N$  eigenvalues  $m$  for an  $N$ -qubit Hamiltonian (details in supplementary material). We observe that the function  $\phi_{QH}$  represents the real-part of a sum over an exponential number of holomorphic functions (the exponentials, with coefficients tuned by circuit parameters  $\theta_1$  and  $\theta_2$ ), and is therefore in total harmonic.

Following the above recipes guarantees the resulting parametrized networks to be harmonic. However, is it not the case that such networks span the space of all harmonic functions. Only harmonic functions on simply connected domains can be written as the real part of a holomorphic function [56]. Recall that a simply connected domain is one where any path between two fixed points can be continuously deformed into any other path connecting the same points. Domains which are not simply connected are referred to as multiply connected. For such domains, we present an alternative approach.

## 2.2 Exact-Harmonicity: Multiholomorphic Networks on Multiply Connected Domains

For many problems of interest, harmonic functions on multiply connected domains need to be constructed. We refer to our networks in these scenarios as multiholomorphic networks, both because they operate on multiply connected domains and because they comprise of multiple (Q)NNs.

We consider a multiply connected domain in  $\mathbb{R}^2$  which we denote by  $\Omega$  and disjointly decompose it such that  $\Omega = (\bigcup_i \omega_i) \dot{\cup} (\bigcup_{i,j} \partial\omega_{i,j})$  with  $i, j \in \mathbb{N}$ , each  $\omega_i$  being simply connected and each  $\partial\omega_{i,j}$  representing a zero-area boundary between the subdomains  $\omega_i$  and  $\omega_j$ .

For each  $\omega_i$ , we associate a (quantum) harmonic neural network  $\phi_H^{(i)} \in \{\phi_{CH}^{(i)}, \phi_{QH}^{(i)}\}$  of the form outlined in Eq. 2 or 3b. We can then construct a representation for a harmonic neural network  $\phi_{MH} : \Omega \rightarrow \mathbb{R}$  as follows:

$$\phi_{MH}(\mathbf{x}) = \begin{cases} \phi_H^{(i)}(\mathbf{x}) & \mathbf{x} \in \omega_i \\ \frac{\phi_H^{(i)}(\mathbf{x}) + \phi_H^{(j)}(\mathbf{x})}{2} & \mathbf{x} \in \partial\omega_{i,j}. \end{cases} \quad (5)$$

While  $\phi_{MH}$  is harmonic by construction on each  $\omega_i$ , it remains to make it harmonic across each  $\partial\omega_{i,j}$ . We achieve this by including an extra loss term  $L_{\partial\omega}$  alongside any other loss that  $\phi_{MH}$  is being optimised upon:

$$L_{\partial\omega} = \sum_{i,j} \mathbb{E}_{\mathbf{x} \sim \partial\omega_{i,j}} \left[ \left( \phi_H^{(i)}(\mathbf{x}) - \phi_H^{(j)}(\mathbf{x}) \right)^2 + \left\| \nabla \phi_H^{(i)}(\mathbf{x}) - \nabla \phi_H^{(j)}(\mathbf{x}) \right\|_2^2 \right], \quad (6)$$

where the first term in the sum incentivises continuity in the harmonic function, and the second term represents a squared  $L_2$  norm which incentivises continuity in the conservative field of the harmonic function. Such a stitching together of domains, with loss-functions ensuring continuity of relevant dynamics, is closely-related to some domain decomposition techniques in PINNs [38].

The fundamental result of such a decomposition is that  $\phi_{MH}$  can be harmonic everywhere, but it need not correspond to any holomorphic function on each  $\partial\omega_{i,j}$ . Since this construction is only non-harmonic on boundaries, we consider it to be harmonic almost everywhere. We consider the practical ramifications of this in Sect.3.5.

## 2.3 Approximate-Harmonicity: Curl-driven Harmonic Networks

We can write Laplace's equation as  $\nabla \cdot (\nabla \phi) = 0$ . This demonstrates that the gradient of any harmonic function must be divergence-free. Furthermore, in three dimensions, a general divergence-free field can be obtained by the identity  $\nabla \cdot (\nabla \times A) = 0$ . This motivates the construction of an inductive bias comprising of two networks:  $\phi_C(\mathbf{x}; \boldsymbol{\theta}_\phi)$  representing the potential field and  $A(\mathbf{x}, \boldsymbol{\theta}_A)$  representing a neural network whose curl will be taken to provide a representation of the underlying conservative field of a harmonic function, where  $\boldsymbol{\theta}_\phi$  and  $\boldsymbol{\theta}_A$  represent trainable parameters. Including the following loss term during network optimisation thus provides an inductive bias towards harmonic functions:

$$L_c(\boldsymbol{\theta}_\phi, \boldsymbol{\theta}_A) = \mathbb{E} \left[ \left\| \nabla \phi_C - \nabla \times A \right\|_2^2 \right] \quad (7)$$

where the expectation is taken with respect to a distribution over which the inductive bias is desired.

Even though the curl operator is only well-defined in three-dimensions, we note that we can use the exterior calculus of differential forms to derive similarly divergence-free operators in arbitrary dimensions. We provide an overview of such derivations in the supplementary material. However, in short, in an  $N$ -dimensional space, we can represent a general  $(N - 2)$ -form with a neural network. By taking the exterior derivative of this neural network, we construct an  $(N - 1)$ -form which represents a divergence-free field. This follows because 1. There is a direct correspondence between the exterior-derivatives of  $N - 1$  forms and the divergence-operator 2. Nested exterior derivatives evaluate to zero by Poincaré’s lemma.

In two-dimensions, this leads (with some abuse of notation in reusing the curl symbol) to:

$$\nabla \times A = \left( \frac{\partial y_1}{\partial x_2}, -\frac{\partial y_1}{\partial x_1} \right), \quad (8)$$

with  $A : \mathbb{R}^2 \rightarrow \mathbb{R}$  defined by  $A(x_1, x_2) = y_1$ . A sample four-dimensional calculation is demonstrated in the supplementary material.

We note that such operators are amenable for implementation on quantum circuits. Two independent quantum circuits representing  $\phi_C$  and  $A$  appearing in Eq. 7 (as well as determining additional loss contributions detailed in Sect. 3.1) can be estimated via simple cost functions (e.g. the *total magnetization*). Composing such contributions into the relevant loss term(s) can be attained by invoking additional classical automatic differentiation routines, e.g. [63]. The latter ones can also handle circuit derivatives (here necessary up to the 2<sub>nd</sub> order), which can be alternatively attained with analytical methods on quantum hardware, such as the parameter-shift rule [15, 64].

### 3 Applications

We exemplify our approaches on four sample applications geared towards electrostatics (Sect.3.3), heat distribution (Sects.3.4&3.5), and robot navigation (Sect.3.6). We provide an independent benchmark in terms of finite element methods (FEM), and assume it as the ground truth in absentia of analytical solutions. In addition to the methods introduced in this work, we also include comparisons to PINNs [5], as well as PINNs with Dirichlet-condition constrained architectures [6]. Full finite elements and classical NN code can be found in the supplementary material. We continue by outlining some loss functions we use with different methods, as well as summarising the implementation of each method.

#### 3.1 Methods

**Dirichlet Losses** Imposing Dirichlet boundary conditions can be done variationally, using mean squared error losses. Given a Dirichlet boundary  $\Gamma$ , where the target function is known to take constant value  $c \in \mathbb{R}$ , we train an arbitrary



(quantum or conventional neural network)  $\text{NN}(\mathbf{x}, \boldsymbol{\theta})$  to obey such a condition by including a term:

$$L_d = \mathbb{E}_{\mathbf{x} \sim \Gamma} \left[ (\text{NN}(\mathbf{x}, \boldsymbol{\theta}) - c)^2 \right] \quad (9)$$

**Physics-Informed Harmonic Losses** Given a spatial-domain  $\Omega$  and a (quantum) neural network  $\text{NN}(\mathbf{x}, \boldsymbol{\theta})$ , we follow established methodologies [5] to define a physics-informed loss towards harmonic functions by zeroing the Laplacian

$$L_{\text{PI}_H} = E_{\mathbf{x} \sim \Omega} \left[ (\nabla^2 \text{NN}(\mathbf{x}, \boldsymbol{\theta}))^2 \right] \quad (10)$$

**Dielectric Interface Loss** To model the behaviour of a potential field across a dielectric interface, we must impose Maxwell’s interface conditions, namely that potential fields (i.e. harmonic functions) are continuous across the interface, and that the normal components of underlying electric fields (i.e. the gradient of the harmonic function) are scaled according to material permittivities [65]. Consequently, given two domains  $\Omega_1, \Omega_2$  with permittivities of  $\epsilon_1$  and  $\epsilon_2$  and (quantum) neural networks  $\text{NN}_1(\mathbf{x}; \boldsymbol{\theta}_1)$  and  $\text{NN}_2(\mathbf{x}; \boldsymbol{\theta}_2)$  defined on each domain respectively, we construct a normal unit vector  $\mathbf{n}(\mathbf{x})$  to the boundary  $\partial\Omega$  between  $\Omega_1$  and  $\Omega_2$  and define the following loss term:

$$L_{\text{PI}_{\text{DE}}}(\boldsymbol{\theta}_1, \boldsymbol{\theta}_2) = E_{\mathbf{x} \sim \partial\Omega} \left[ (\text{NN}_1(\mathbf{x}; \boldsymbol{\theta}_1) - \text{NN}_2(\mathbf{x}; \boldsymbol{\theta}_2))^2 + \left( \epsilon_1 \frac{\partial E_1}{\partial \mathbf{n}} - \epsilon_2 \frac{\partial E_2}{\partial \mathbf{n}} \right)^2 \right] \quad (11)$$

where  $E_i$  represents the electric field in domain  $\Omega_i$ . In general contexts, we have  $E_i = \nabla \text{NN}_i(\mathbf{x}, \boldsymbol{\theta})$ . However, in the case of our curl-based approach, we represent  $E_i$  by the underlying divergent free field  $\nabla \times A$  as outlined in Sect. 2.3.

**(q)PINN** We define a single (quantum or conventional) neural network,  $\phi_{\text{PINN}}(\mathbf{x}; \boldsymbol{\theta})$  and minimise the loss

$$L_{\text{PINN}} = L_{\text{PI}_H} + L_d \quad (12)$$

with  $L_{\text{PI}_H}$  and  $L_d$  defined in Eqs. 9 and 10 respectively.

**h(q)PINN** Given a multilayer perceptron  $\text{MLP}(\mathbf{x}; \boldsymbol{\theta})$  and a Dirichlet boundary  $\Gamma$  taking constant value  $c \in \mathbb{R}$  on it, we can construct a neural network that exactly satisfies the boundary condition while leaving flexibility to optimise towards harmonic functions [6]. First, we define a distance function  $d(\mathbf{x})$  representing the shortest distance between a generic point  $x \in \Omega$  and  $\Gamma$ , and then define a neural network of the form:

$$\phi_{\text{hPINN}} = ce^{-kd(\mathbf{x})} + (1 - e^{-kd(\mathbf{x})})\text{MLP}(\mathbf{x}; \boldsymbol{\theta}), \quad (13)$$

where  $k \in \mathbb{R}$  is a hyperparameter to be chosen. Since this network satisfies Dirichlet condition automatically, it can be trained by optimising on Eq. 10 directly.

**Holomorphic** We construct a harmonic neural network as defined in Eq. 2 and a harmonic quantum neural network as defined in Eq. 3b. Since these networks are harmonic by construction, our task of training them is reduced to a supervised learning problem on the boundary terms/data. Consequently we train them by minimising Eq. 9 alone.

**Curl(q)Net** We define two neural networks  $\phi_c(\mathbf{x}, \boldsymbol{\theta}_1)$  and  $A(\mathbf{y}, \boldsymbol{\theta}_2)$  as outlined in Sect.2.3. Note that  $\nabla\phi_c$  and  $\nabla \times A$  must operate in the same space, however in general the two (q)NNs can be defined on different spaces.

The Curl(q)Net solution is achieved by minimising the following objective function:

$$L_{\phi_c} = L_d + L_c \quad (14)$$

with  $L_d$  and  $L_c$  defined in Eqs. 9 and 7 respectively. Indeed, satisfying  $L_c$  amounts to satisfy  $L_{PI_H}$ . We substitute Eq. 8 into 7 in our scenario, since our applications are in two-dimensions. We further note that the term  $L_d$  can be dropped from the optimisation procedure if  $\phi_c$  is defined in a manner analogously to Eq. 13.

**Multiholomorphic** In the case of multiply connected domains, we decompose the domain into simply connected components so that we can still leverage holomorphic function to derive harmonic neural networks (see also Fig. 2a). Thus, we take a multiholomorphic network  $\phi_{MH}$  as defined in Eq. (5) and minimise the following:

$$L_{MH} = L_{\partial\omega} + L_d \quad (15)$$

with  $L_d$  and  $L_{\partial\omega}$  defined in Eqs. 9 and 6 respectively.

**XPINN** Since our multiholomorphic function involves partitioning a domain, we include a domain decomposition strategy applied to PINNs as a further benchmark to try and maintain a fair perspective. The fundamental idea behind XPINNs, is to decompose a domain into disjoint subdomains [38], whilst variationally inducing the continuity of the solutions across each subdomain. We can define a neural network  $\phi_{XPINN}(\mathbf{x}; \boldsymbol{\theta})$  analogously to the multiholomorphic network in Eq. 5, except we use real-valued multilayer perceptrons on each subdomain as opposed to harmonic neural networks. Consequently we can train  $\phi_{XPINN}(\mathbf{x}; \boldsymbol{\theta})$  by minimising

$$L_{XPINN} = L_{\partial\omega} + L_d + L_{PI_H}, \quad (16)$$

with  $L_{\partial\omega}$ ,  $L_d$  and  $L_{PI_H}$  defined in equations 6, 9 and 10 respectively, the latter contribution being necessary due to dropping of conditions imposing harmonicity.

### 3.2 Experimental Setup

We conduct all (both quantum and conventional) experiments in Python3 and make use of NumPy [66] and Matplotlib [67]. FEM ground truths were constructed using FeniCS [68]. Hardware specifics are in the supplementary material.

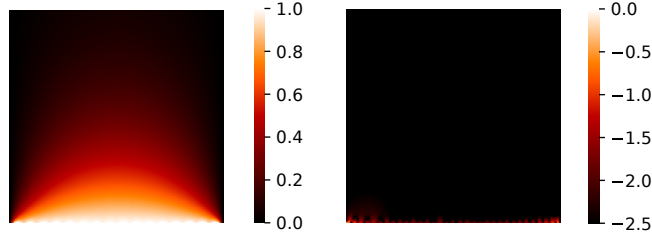


Figure 1: (Left) heat profile - in arbitrary units - for a refrigerated unit-sized box with the bottom side heated, computed with a numerical simulation of a 4 qubits hQNN. (Right)  $\log_{10}$ -scale error of the hQNN vs analytical solution.

**Conventional Machine Learning** We implement all neural networks in PyTorch [69]. We consistently use multilayer perceptrons with 3 hidden layers, width 32, initialised with Kaiming Uniform initialisers [70], optimised for 16,000 epochs over full-batches with an Adam optimizer [71] with a learning rate (LR) of  $10^{-3}$ . We use tanh activations for real-valued NNs and sin activations for holomorphic NNs. For each application, we construct boundary conditions comprising of lines where we sample 100 uniformly-spaced points. To minimise physics-informed losses, we sampled 1024 collocation points randomly (uniformly) on the interior of each domain. These points are sampled once and then kept constant for each experiment to allow each run the same amount of information.

**Quantum Machine Learning** All the QNNs used in this paper are implemented with proprietary code, leveraging upon the packages PyTorch and Yao.jl [72]. Details of the various components introduced in this paragraph can be found in [18]. We consider two types of QNNs: for the first, of type (3a) with  $|\Psi_{\theta,x,y}\rangle = \hat{\mathcal{U}}_{\theta_2} \text{QFM}(x,y) \hat{\mathcal{U}}_{\theta_1} |\emptyset\rangle$ , we choose to decompose the QFM as two parallel *Chebyshev-tower* QFM's that apply a  $Y$  rotation gate, each spanning 4 qubits. These encoding gates are sandwiched between two layers of variational blocks: a pair of parallel 4-qubit variational blocks before, and a single 8-qubit block after the QFM. All variational blocks employ **CNOT** entangling gates interleaved with single-qubit parametrized rotations. The training was performed by a hybrid optimization scheme comprising 1200 epochs of Adam [71], followed by 300 epochs of L-BFGS [73], both with learning rate 0.05. To extract information at the end of the evolution, we employ the total magnetization operator. The overall circuit diagram is illustrated for clarity in the supplementary material. The second QNN that we use is the quantum harmonic neural network of type (3b) with a complex-exponential QFM,  $N=4$  qubits, and VB's  $\hat{\mathcal{U}}_{\theta_k}$  with depths 8 for both  $k = \{1, 2\}$ .

Table 1: Performance of our methods on the electrostatic benchmark illustrated in Sect. 3.3. We present the mean and standard deviation of each method over 10 repeated runs. In addition, we report the expected absolute Laplacian over the spacial domain, which should be identically zero for perfectly harmonic functions. We separate quantum (see also Fig. 2) and conventional techniques with a horizontal line. Lower numbers indicate better performance. Entries are sorted in order of ascending mean RMSE.

<i>Electrostatic</i> bench.	mean RMSE	std RMSE	mean $E[ \nabla^2\phi ]$	std $E[ \nabla^2\phi ]$
Holomorphic (ours)	3.29e-03	8.53e-04	0.00e+00	0.00e+00
CurlNet (ours)	1.40e-02	6.36e-04	1.65e+00	2.73e-01
PINN	6.72e-02	1.78e-02	5.30e-02	5.74e-03
hPINN	9.99e-02	2.94e-04	1.14e-01	1.26e-02
CurlqNet (ours)	3.38e-02	3.29e-04	2.69e+00	1.54e-01
qPINN	1.38e-01	2.80e-03	8.47e-02	6.55e-03
hqPINN	1.62e-01	1.84e-02	1.01e-01	1.97e-01

### 3.3 Results A: Dielectric material in a charged box

Consider a dielectric material placed in a 2D box grounded on 3 sides, and an electric potential applied to the bottom edge. We consider the task of inferring the underlying electric potential field within the box, in the presence of different materials.

We thus introduce a first dielectric domain  $\Omega_1 = [0, 1] \times [0, 0.5]$ , with permittivity  $\epsilon_1 = 1.0$  and free-space above the dielectric as  $\Omega_2 = [0, 1] \times [0.5, 1]$  with permittivity  $\epsilon_2 = 0.01$ . The bottom lid ( $y = 0$ ) has an applied voltage of  $V = 1.0$  (in arbitrary units), whereas  $V = 0.0$  on all other boundaries. We define neural networks and losses on each  $\Omega_1$  and  $\Omega_2$  as outlined in Sect. 3.1. In addition, we couple the losses of both networks using Eq. 11 and optimize both networks jointly. We do not consider our multiholomorphic or the XPINN architecture in this scenario, since they were devised for use on multiply connected domains, as opposed to the simply connected setting in this application.

We report in Table 1 the results as (i) root mean squared errors (RMSE) against FEM solutions, i.e.  $\sum_{\mathbf{x}_i \in \tilde{\Omega}} \sqrt{(\phi(\mathbf{x}_i) - \phi_{\text{FEM}}(\mathbf{x}_i))^2} / |\tilde{\Omega}|$ , where  $\tilde{\Omega} \equiv \{\mathbf{x}_i\}$  a set of collocation points uniformly sampled in the interior domain  $\Omega$ , along with (ii) the expected absolute Laplacian over  $\Omega$ .

We note that PINNs achieve a low mean Laplacian over the domain, even though they do not represent the best performing solutions. One possible explanation would be that the Laplacian is directly optimised for PINNs (equations 10 and 12), but minimising such a loss could still lead to systematic errors across a spatial domain.

Table 2: Performance of our methods on the heat-distribution benchmark illustrated in Sect. 3.5. Details are the same as for Table 1

<i>Heat distrib. bench.</i>	mean RMSE	std RMSE	mean $E[ \nabla^2\phi ]$	std $E[ \nabla^2\phi ]$
Multiholomorphic (ours)	2.44e-03	8.84e-04	0.00e+00	0.00e+00
XPINN	2.40e-02	2.38e-04	1.11e-03	2.89e-03
hPINN	2.41e-02	5.82e-05	2.92e-04	4.65e-04
PINN	2.41e-02	5.78e-06	1.58e-05	3.43e-06
CurlNet (ours)	2.41e-02	4.27e-05	4.01e-04	4.78e-04
Holomorphic (ours)	1.91e-01	5.36e-04	0.00e+00	0.00e+00
CurlqNet (ours)	2.14e-02	2.13e-04	2.83e-02	3.92e-03
hqPINN	6.52e-02	3.89e-04	2.40e-02	4.91e-03
qPINN	1.72e-01	3.14e-03	2.82e-01	2.38e-02

### 3.4 Results B: Heat distribution in a box with single-sided heating

We consider a refrigerated square box with uniform heating on a single side, where we wish to find the steady-state heat distribution described by  $\phi$ . We consider a domain  $\Omega = [0, 1] \times [0, 1]$ . Desired Dirichlet boundary conditions are  $\phi = 1$  on the edge  $x = 0$ , and  $\phi = 0$  (in arbitrary units) when  $y = 0$ ,  $y = 1$ , or  $x = 1$ . Note that this problem is a single (simply-connected) domain. We know the analytical solution as an infinite series, and plot the converged result as well as the absolute error with the analytical result in Fig. 1. With 4 qubits and an exponential-spectrum QFM, the hQNN is able to represent up to  $2^4 = 16$  basis functions, and we find many similarities between the analytical series cut to the first 16 terms and the converged hQNN (see also the supplementary material); we predict an exponential expressivity for these types of hQNN in solving Laplace’s equation, with a potential advantage over classical NN’s.

### 3.5 Results C: Heat distribution around heater

We consider a heated triangular body in a refrigerated box, where we wish to find the steady-state heat distribution described by  $\phi$ .

We consider a domain  $\Omega = [0, 10] \times [0, 10]$ , with an equilateral triangle of length 4 centred in the box as illustrated in Fig. 2a. Desired Dirichlet boundary conditions are  $\phi = 1$  on the triangle edges and  $\phi = 0$  (in arbitrary units) when  $x = 0$ ,  $x = 10$ ,  $y = 0$  or  $y = 10$ . With these conditions,  $\phi$  defines a harmonic function representing the steady-state temperature distribution inside the box.

Note that this problem is not on a simply-connected domain. For example, a closed path around the triangular body cannot be reduced to a point, without crossing the body. Consequently, we have reason to believe that the resulting solution will not be representable by our holomorphic formulation, though it could be representable by a multiholomorphic formulation. We partition our domain as outlined in Fig. 2a for both XPINN and multiholomorphic approaches, and report our results in Table 2. Note that as in section 3.3, we note that a low expected absolute Laplacian does not necessarily correspond to a good solution

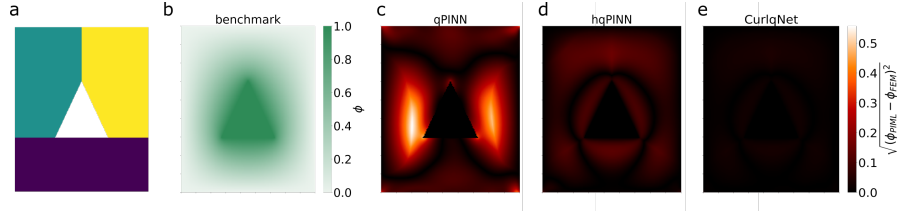


Figure 2: (a) A partitioning of the multiply connected domain in Sect.3.5 into three simply connected domains on which we define our multiholomorphic and XPINN networks. Note that the white triangle in the centre is not considered a part of the domain. (b) The solution  $\phi(x, y)_{\text{FEM}}$  of the problem of a triangular heater positioned in a square box with Dirichlet boundary conditions, as provided by a FEM solver for benchmark. (c-e) A comparison of the performance for different QNN architectures, by plotting the RSE when comparing against  $\phi(x, y)_{\text{FEM}}$  the solution  $\phi(x, y)_{\text{PIML}}$  provided respectively by (c) a naïve (qPINN), (d) an hqPINN and a (e) CurlqNet architectures. Additional details and definitions are provided in the main text. All plots report a sample of the reference metric on a uniform  $150 \times 150$  grid. Points within the subdomain belonging to the heater have been excluded from the analysis.

in terms of RMSE. All the figures of merit for this case are equivalent to those outlined in Sect. 3.3.

### 3.6 Results D: Robot Navigation in a previously explored environment

We consider a robot navigating a known, static environment, e.g. a pre-explored corridor. The use of general potential to guide robot movement is well-established, and it can present evident advantages over traditional path-finding algorithms [74]. For example, it offers a symbolic, parameterized representation of the environment that can be easily updated with new information, as well as exploiting special properties of the mechanical system to ensure a more stringent adherence to problem constraints, such as e.g. a maximum available torque to the robot. In particular, it was noted later that harmonic functions have favourable properties for robot navigation [75]. Namely, harmonic functions do not attain local minima anywhere (except for constant harmonic functions), corresponding to virtually preventing the robots from becoming stuck. This property led to a few dedicated studies [76, 77].

Define a domain  $\Omega = ([0, 0.5] \times [0, 0.6]) \cup ([0.5, 1.0] \times [0.4, 1.0])$ . We construct a harmonic function,  $\phi$  with Dirichlet boundary conditions  $\phi = -1$  at  $y = 0$  and  $\phi = 1$  at  $y = 1$  and compare CurlNet, Holomorphic and PINNs in Fig.3.

We note that even though the holomorphic network did not characterise the underlying potential field as accurately as the CurlNet, it provided the most consistent robot navigation paths. This might be explained from the high errors

in Laplacian measured in the CurlNet approach. The latter is observable also in the CurlqNet, even though to a lesser extent.

See Table 3 for a full comparison of mean squared errors in the potentials and Laplacian’s over valid points (i.e. within the environment accessible to the robot) extracted from a uniform  $64 \times 64$  grid, for both classical methods and their previously introduced quantum counterparts. Finally, we observe how in general quantum implementations deliver more consistent results across independent runs (with a fixed architecture of the quantum circuit).

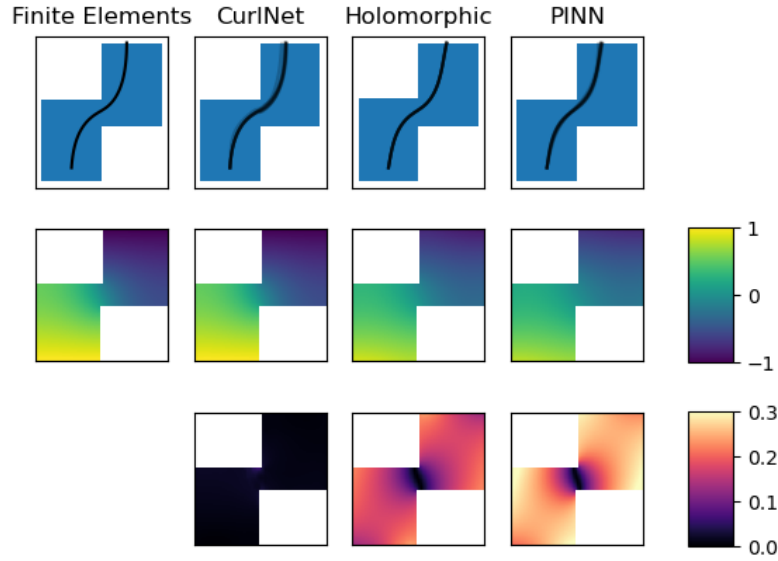


Figure 3: Figures generated from the robot navigation task in Sect.3.6 over 10 different network initialisations. First row: robot navigation paths overlapped, with visualization of the domain. Second row: the potential  $\phi$  generated to guide the robot, as averaged over the 10 exemplary runs. Third row: the absolute error between the potential  $\phi$  generated for each method, and the corresponding finite elements solution. First column: the reference finite element results, second-to-fourth columns: the results attained with the corresponding neural architectures.

## 4 Discussion

Constructing inductive biases towards various applications has been a key driver of recent progress in classical machine learning, whereas it is still a nascent field

Table 3: Performance of our methods on the robot navigation benchmark illustrated in Sect. 3.6. Details are the same as for Table 1

<i>Navigation</i> bench.	mean RMSE	std RMSE	mean $E [ \nabla^2 \phi ]$	std $E [ \nabla^2 \phi ]$
CurlNet (ours)	1.56e-02	1.13e-02	20.13e+00	15.02e-00
Holomorphic (ours)	1.71e-01	4.69e-03	0.00e+00	0.00e+00
PINN	2.42e-01	2.81e-01	1.12e-01	1.79e-02
CurlqNet (ours)	6.60e-02	8.90e-04	3.07e+00	9.35e-02
qPINN	3.30e-01	3.86e-03	1.43e-01	5.61e-03

for quantum circuits. In this work we demonstrated the inclusion of inductive biases in classical and quantum neural networks alike towards harmonic functions, observing how despite their crucial importance, there had been only few attempts at including specifically harmonic inductive biases. In summary, we constructed exactly harmonic functions in two-dimensions in simply connected domains, harmonic functions almost everywhere in two-dimensional multiply connected domains, and approximately harmonic functions in arbitrary domains. We demonstrated our approach with comparisons to (quantum) physics-informed neural networks [5, 18] in a range of tasks, namely heat distribution, electrostatics and robot-navigation. Previous tools in this domain were mostly limited to finite-element modelling [4], which is less suited for problems such as inverse-design and transfer learning. Training upon conventional neural networks as well as simulated quantum circuits confirmed the benefits of our newly proposed architectures. Interestingly, we note that achieving a low Laplacian in a given solution is not always consistent with achieving low mean squared errors against a trustworthy benchmark. It is perhaps unsurprising that PINNs typically have low differential equation residuals when trained, since they optimise against PDE residuals directly. However, it is interesting that this might not necessarily be the best strategy to achieving a low error in the resulting solution, as evidenced by the fact that our CurlNet architectures consistently achieve lower RMSEs than their PINN counterparts, whilst exhibiting higher errors in their Laplacians. Beside the merits in all those applications where harmonic functions are relevant, our work highlights how developments in conventional machine learning architectures can be sometimes readily ported in the corresponding realm of quantum machine learning, here exemplified by trainable, parameterised quantum circuits architectures. We hope that our findings encourage further cross-pollination between the quantum and classical machine learning fields.



## Supplementary Material

### A Holomorphic Quantum Circuits and Harmonic Quantum Neural Networks

Our aim is to construct quantum circuits which exhibit holomorphic properties. In a general form, a QNN model can be written as

$$\phi_Q(\mathbf{x}) = \langle \emptyset | \hat{\mathcal{U}}(\mathbf{x}, \boldsymbol{\theta})^\dagger \hat{\mathcal{H}}(\mathbf{x}, \boldsymbol{\theta}) \hat{\mathcal{U}}(\mathbf{x}, \boldsymbol{\theta}) | \emptyset \rangle, \quad (17)$$

where the unitary circuit ansatz  $\hat{\mathcal{U}}(\mathbf{x}, \boldsymbol{\theta})$ , and the Hermitian cost Hamiltonian  $\hat{\mathcal{H}}(\mathbf{x}, \boldsymbol{\theta})$ , are functions of function-input variables and model parameters  $\boldsymbol{\theta}$ , and  $|\emptyset\rangle$  represents the 0-state, i.e. a reference state for the quantum computation. Alternatively, a different type of quantum model can be written as

$$\phi_{QH}(\mathbf{x}) = \Re \langle \emptyset | \hat{\mathcal{U}}(\mathbf{x}, \boldsymbol{\theta}) | \emptyset \rangle, \quad (18)$$

which represents the real part of a complex number obtained from measuring the overlap of the parametrized state (i.e. the reference 0-state evolved by the unitary  $\hat{\mathcal{U}}$ , for example prepared on a register of qubits), with the 0-state itself. Such overlap can be computed using e.g. the Hadamard or SWAP tests [78]. To compute the value of  $\phi_Q(\mathbf{x})$  or  $\phi_{QH}(\mathbf{x})$ , or even approximate it, is believed to be very computationally intensive on a classical computer for systems involving large unitaries  $\hat{\mathcal{U}}$  (which in turn corresponds to the size of the target system). On the contrary, this is typically feasible on a quantum computer, provided some assumption on the circuit structure, and eventually the cost Hamiltonian for  $\phi_Q(\mathbf{x})$  [10].

For simplicity and ease of analysis, we here restrict ourselves to a specific structure of the cost Hamiltonian as being independent of  $\mathbf{x}$  and  $\boldsymbol{\theta}$ , i.e.  $\hat{\mathcal{H}}(\mathbf{x}, \boldsymbol{\theta}) = \hat{\mathcal{H}}$ , and the circuit structure as

$$\hat{\mathcal{U}}(\mathbf{x}, \boldsymbol{\theta}) = \hat{\mathcal{U}}_{\theta_2} \text{QFM}(\mathbf{x}) \hat{\mathcal{U}}_{\theta_1}, \quad (19)$$

is then a single quantum feature map  $\text{QFM}(\mathbf{x})$ , squeezed between two general variational circuits  $\hat{\mathcal{U}}_{\theta_j}$  [18] which only depend on model parameters  $\boldsymbol{\theta}_j$ .

To describe a particular type of QFM in the form of a Hamiltonian evolution, we first make use of the following decomposition of a Hamiltonian evolution applied to some arbitrary initial state  $|\Psi_{\text{ini}}\rangle$ :

$$e^{-it\hat{\mathcal{G}}} |\Psi_{\text{ini}}\rangle = \sum_m c_m e^{-itE_m} |\psi_m\rangle. \quad (20)$$

For the examples in our paper  $\mathbf{x} \equiv (x, y)$  - as we only deal with 2D problems - and for a QFM of the form in (20), we can think that the dependency upon the two variables can be expressed via the time:

$$t = t(x, y). \quad (21)$$

Inserting this expression in (17), where  $|\Psi_{\text{ini}}\rangle \equiv |\emptyset\rangle$ , using the assumption (19), and reminding that the decomposition in (20) involves orthonormal  $|\psi_m\rangle$ , which are also eigenstates of  $\hat{\mathcal{G}}$ , i.e.  $\hat{\mathcal{G}}|\psi_m\rangle = E_m|\psi_m\rangle$ , we find:

$$\phi_Q(x, y) = \langle \Psi(\theta_1) | e^{it\hat{\mathcal{G}}} \hat{\mathcal{H}}(\theta_2) e^{-it\hat{\mathcal{G}}} | \Psi(\theta_1) \rangle = \sum_{\langle m, n \rangle} c_{mn}(\theta_1, \theta_2) e^{-it(E_m - E_n)} \quad (22)$$

where  $\hat{\mathcal{H}} = \hat{\mathcal{U}}_{\theta_2}^\dagger \hat{\mathcal{H}} \hat{\mathcal{U}}_{\theta_2}$  indices  $\langle m, n \rangle$  sum over all  $m$  and  $n$  from 1 to the size of the accessible Hilbert space (i.e.  $2^N$  for an N-qubit register). While  $c_{mn}$  are generally complex-valued, the resulting function output is guaranteed to be real-valued.

For a QNN of the form  $\phi_{QH}(x, y)$  we find

$$\phi_{QH}(x, y) = \Re \left\{ \sum_m c_m(\theta_1) \langle \emptyset | \hat{\mathcal{U}}_{\theta_2} | \psi_m \rangle e^{-itE_m} \right\} = \Re \left\{ \sum_m \tilde{c}_m(\theta_1, \theta_2) e^{-itE_m} \right\}. \quad (23)$$

If we now consider a time evolution in (21) of the form  $t(x, y) = y - xi$ , we obtain the result from the main text in Eq. 4. This yields a sum over exponentials of holomorphic functions, which is thus holomorphic itself and has a harmonic real part.

With this choice, we find the quantum models to be represented by linear combinations of  $e^{-(x+iy)E}$  with  $E$  some number representing an eigenvalue, or gap between two eigenvalues, of the QFM evolution Hamiltonian. The number of unique terms is therefore equal to the number of unique (non-degenerate) eigenvalues or gaps in the spectrum of the QFM evolution Hamiltonian. The more unique terms, the more basis functions and thus the more expressivity the quantum model can obtain. We describe here the specific complex-exponential QFM we chose for the results section

$$\text{QFM}(x, y) = e^{(x-iy)\pi\hat{\mathcal{H}}} \quad \text{where} \quad \hat{\mathcal{H}} = \sum_{j=0}^{N-1} 2^j \hat{Z} + 2^N. \quad (24)$$

this Hamiltonian has  $2^N$  unique eigenvalues  $E_m = 2m - 1 = \{1, 3, 5, 7 \dots (2 \cdot 2^N - 1)\}$ .

### A.1 Applying harmonic QNNs to solve an instance of the Laplace Equation

In the main paper, Sect. 4.4 (Results B), we considered the solution of the Laplace equation for the heat distribution  $f(x, y)$  inside a unit-square box refrigerated on all sides (where then the Dirichlet b.c. applicable impose  $f|_{\partial\Omega_{1-3}} = 0$ ) but one (occurring at  $x = 0$ ), where we assume the presence of a heater, modelled by imposing a Dirichlet b.c.  $f|_{\partial\Omega_4} = 1$ .

The general solution to this problem setting is known in closed-form as a series expansion

$$f(x, y) = \sum_{n \text{ odd}}^{\infty} \frac{4}{n\pi} e^{-n\pi x} \sin(n\pi y) = \frac{2}{\pi} \arctan \frac{\sin(\pi y)}{\sinh \pi x} \quad (25)$$

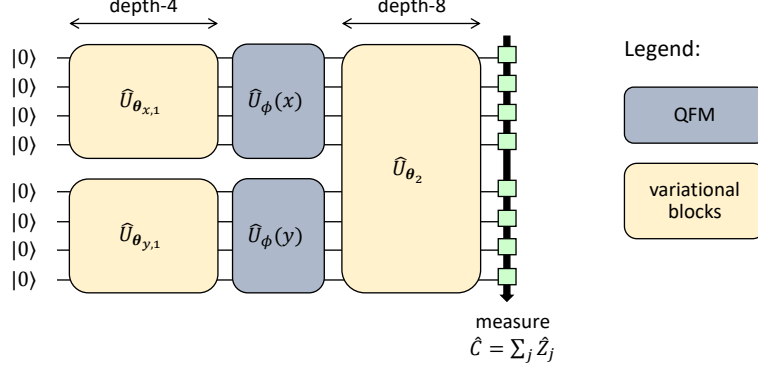


Figure 4: The overall 8-qubit QNN circuit structure, employed as described in Sect. 3.2 of the main paper. Further details on the Quantum Feature Map (QFM) and (hardware-efficient) variational blocks can be found in [18].

The exact solution can thus also be numerically approximated; as the coefficients become smaller with the term index, by truncating the sum to a given number of terms  $\tilde{N}$ , the solution becomes closer and closer to exact. We note that expansions equivalent to (25) exist also for cases where  $f|_{\partial\Omega_4} = f(y)$ , and for the general case of a 2D Laplace equation with Dirichlet b.c., it is expected that alternative expansions can naturally approximate the solution. However, in general, the analytical function representation of the series is not always known, and therefore numerical truncation methods are the best alternative. Having access to a large number of terms improves the approximation.

In Fig. 5 we plot the converged results and the loss convergence profile for a QNN adopting  $N = 4$  qubits. We find the solution matches very well overall, with only a slight deviation at the  $x = 0$  boundary, for all  $y$ , with clear oscillatory behaviour. This can be explained by the so-called Gibbs phenomenon, which is a demonstration that step-function behaviour can in principle be modelled accurately with periodic functions, but the amplitude error remains significant even for larger cut-off in the series. The step-function is required by the sharp transition  $\lim_{y \rightarrow 0^+} f(x = 0, y) = 1$  whilst  $\lim_{y \rightarrow 0^-} f(x = 0, y) = 0$ , which occurs at the corners of the unit-box for  $x = 0$  due to the discontinuous b.c. imposed.

We observe very similar profiles (results omitted) for the solution represented by a finite sum, with a cut-off at 16 terms. This confirms the intuition about the hQNN expressivity outlined in the last paragraph: the  $N = 4$  case employs  $2^N = 16$  terms, so that we expect a performance similar to expressing the solution by introducing the same number of terms in (25) - where the coefficients of the terms are fixed and not variationally optimised. This intuitive reasoning signifies the capacity of the hQNN to represent basis functions to the Laplace

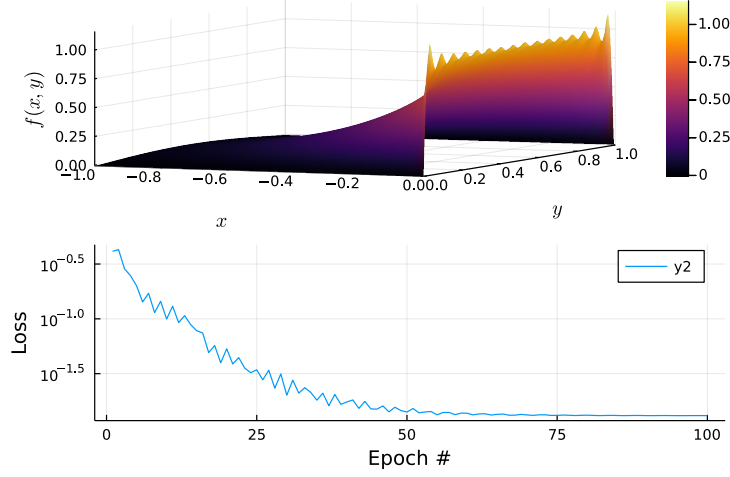


Figure 5: (Top) Converged QNN output for solving Laplace’s equation on a unit square domain with boundary conditions setting three sides to  $f(x, y) = 0$  and one side to  $f(x, y) = 1$ . (Bottom) Loss profile as a function of epoch # in the QNN training process.

problem.

Finally, we stress how the hQNN converges very rapidly to the approximate solution, in less than 100 epochs.

## A.2 Quantum Imaginary- and Complex-Time Evolution

So-far we have assumed we can directly substitute a complex number into the  $t$  variable representing time evolution over a Hamiltonian. But how would one implement complex-time evolution in a real quantum system? In this section, we will highlight strategies known in literature as Quantum Imaginary Time Evolution (QITE) and extend these to general Quantum Complex Time Evolution (QCTE).

QITE is a strategy that was first used in classical computing, in particular in the field of computational quantum chemistry, to prepare ground-states/energies for certain types of Hamiltonians, including molecular and lattice Hamiltonians. More recently, it was shown that quantum algorithms could offer a substantial speedup over classical methods. There are many variations of QITE, but two main approaches are the Trotterized-version by Motta et al. [61] and the variational approach described by McArdle et al. [59].

In Motta et al. [61], the overall imaginary time evolution step is expanded into a series of Trotter steps. Each step evolves over only a very short time. Based on locality properties, one can construct an approximate linear system that is solved on a classical computer to find a proxy unitary operator that can replace the non-unitary step, including the appropriate normalization factor. In

our work, that normalization factor would be re-multiplied as a scalar number in classical post-processing to capture a desirable decaying effect.

Because the proposal is already based on a Trotterization-approach, it is possible to show that the QITE can be extended to QCTE by interleaving imaginary-time-evolution Trotter steps with real-time-evolution Trotter steps as

$$e^{-\beta(\hat{H}_r + i\hat{H}_i)} = (e^{-\Delta\tau\hat{h}_r[1]}e^{-i\Delta\tau\hat{h}_i[1]}e^{-\Delta\tau\hat{h}_r[2]}e^{-i\Delta\tau\hat{h}_i[2]}\dots)^n + \mathcal{O}(\Delta\tau) \quad (26)$$

where we decomposed both  $\hat{H}_r$  and  $\hat{H}_i$  into sums of mutually commuting operators  $\hat{h}_r[m]$  and  $\hat{h}_i[m]$  respectively, and  $n = \frac{\beta}{\Delta\tau}$ .

McArdle et al. [59] aims to circumvent the impractical circuit depth requirements of [61] by taking an approximate, variational approach, now also referred to as VarQITE (Variational QITE). McLachlan’s variational principle is used to map the imaginary-time evolved states onto a suitable, chosen variational ansatz, allowing to effectively perform QITE on a quantum device. Also in this case, QCTE proposes to replace the real Hamiltonian term by a more general complex Hamiltonian. However, future work would still be required to adapt the VarQITE estimate routine of the normalization factor to our case.

## B Divergence free (quantum) neural networks

We use exterior derivatives on differential forms to construct divergence-free networks in arbitrary dimension. To construct divergence-free networks in an  $N$ -dimensional space, we can represent a general  $(N - 2)$ -form with a neural network. Taking the exterior derivative of this network yields a divergence-free  $(N - 1)$ -form. This follows since 1. There is a correspondence between the exterior derivatives of  $(N - 1)$ -forms and divergence operators. 2. Nested exterior derivatives evaluate to zero by Poincaré’s Lemma. A full treatment of differential forms lies outside the scope of this work (see e.g. [79, 80] for more detailed coverage), so we focus instead on practical demonstrations aimed to facilitate the derivation of divergence-free neural networks in further work.

### B.1 Two dimensions

While divergence-free fields in two dimensions might be constructed by inspection, we use the two dimensional case as a showcase of the methodology involving differential forms.

Start with the definition of a general zero-form:

$$f = y(x_1, x_2), \quad (27)$$

on which we take an exterior derivative:

$$df = \frac{\partial y}{\partial x_2} dx_2 + \frac{\partial y}{\partial x_1} dx_1. \quad (28)$$

Consider an exterior derivative on a general 1-form  $g = adx_2 - bdx_1$ :

$$dg = \left( \frac{\partial a}{\partial x_1} dx_1 + \frac{\partial a}{\partial x_2} dx_2 \right) dx_2 - \left( \frac{\partial b}{\partial x_1} dx_1 + \frac{\partial b}{\partial x_2} dx_2 \right) dx_1 \quad (29)$$

$$= \left( \frac{\partial a}{\partial x_1} + \frac{\partial b}{\partial x_2} \right) dx_1 dx_2, \quad (30)$$

where we use the identity on differential forms that  $dx_i dx_j = -dx_j dx_i$ , which also implies that  $dx_i dx_i = 0$ .

This demonstrates the correspondence between the exterior derivative of an  $(N-1)$ -form and the divergence operator.

Since  $d(d(f)) = 0$  for any differential form  $f$ , equating coefficients between  $df$  and  $g$  then yields a formula for a divergence-free field in two dimensions. So, given a map  $(x_1, x_2) \rightarrow y$ , then the field:

$$\left( \frac{\partial y}{\partial x_2}, -\frac{\partial y}{\partial x_1} \right) \quad (31)$$

is divergence-free.

## B.2 Four dimensions

Since the three-dimensional case is well-handled by standard vector calculus, we turn to four dimensions as a final demonstration of practical calculations of divergence-free fields with differential forms. We note that increasing complexity of these calculations might make them better suited for calculation using a computer algebra system.

We start by defining a general 2-form in four dimensions:

$$f = y_1 dx_1 dx_2 + y_2 dx_1 dx_3 + y_3 dx_1 dx_4 + y_4 dx_2 dx_3 + y_5 dx_2 dx_4 + y_6 dx_3 dx_4. \quad (32)$$

Taking exterior derivatives results in:

$$\begin{aligned} df &= \left( \frac{\partial y_4}{\partial x_4} - \frac{\partial y_5}{\partial x_3} + \frac{\partial y_6}{\partial x_2} \right) dx_2 dx_3 dx_4 \\ &+ \left( -\frac{\partial y_2}{\partial x_4} + \frac{\partial y_3}{\partial x_3} - \frac{\partial y_6}{\partial x_1} \right) dx_3 dx_4 dx_1 \\ &+ \left( \frac{\partial y_1}{\partial x_4} - \frac{\partial y_3}{\partial x_2} + \frac{\partial y_5}{\partial x_1} \right) dx_4 dx_1 dx_2 \\ &+ \left( -\frac{\partial y_1}{\partial x_3} + \frac{\partial y_2}{\partial x_2} - \frac{\partial y_4}{\partial x_1} \right) dx_2 dx_3 dx_4, \end{aligned} \quad (33)$$

where again we use  $dx_i dx_j = -dx_j dx_i$  and  $dx_i dx_i = 0$ .

Considering the exterior derivative of general 3-form  $g = adx_2 dx_3 dx_4 + bdx_3 dx_4 dx_1 + cdx_4 dx_1 dx_2 + ddx_2 dx_3 dx_4$  yields:

$$dg = \left( \frac{\partial a}{\partial x_1} + \frac{\partial b}{\partial x_2} + \frac{\partial c}{\partial x_3} + \frac{\partial d}{\partial x_4} \right) dx_1 dx_2 dx_3 dx_4. \quad (34)$$

Now, equating coefficients between  $df$  and  $g$  yields a divergence-free network in four dimensions, i.e. given six-dimensional map  $(x_1, x_2, x_3, x_4, x_5, x_6) \rightarrow (y_1, y_2, y_3, y_4, y_5, y_6)$  the map

$$\begin{aligned} & \left( \frac{\partial y_4}{\partial x_4} - \frac{\partial y_5}{\partial x_3} + \frac{\partial y_6}{\partial x_2}, \right. \\ & -\frac{\partial y_2}{\partial x_4} + \frac{\partial y_3}{\partial x_3} - \frac{\partial y_6}{\partial x_1}, \\ & \frac{\partial y_1}{\partial x_4} - \frac{\partial y_3}{\partial x_2} + \frac{\partial y_5}{\partial x_1}, \\ & \left. -\frac{\partial y_1}{\partial x_3} + \frac{\partial y_2}{\partial x_2} - \frac{\partial y_4}{\partial x_1} \right). \end{aligned} \tag{35}$$

is divergence-free.

## C Experimental details

The classical neural networks we use are comparatively lightweight, and training for all conventional NNs was done on a single Apple M1 chip running Python 3.9.12 on macOS 12.3.1.

Equivalently, experiments involving QNNs were run on an AMD<sup>©</sup> Ryzen 7 3700x processor, in a Python 3.9.5 Conda environment on Ubuntu 18.04.

Each experiment was repeated 10 times for each method to ensure repeatability of the outcomes, with the attained average values and standard deviation from the mean reported in the main paper tables.

## References

- [1] E. Prestes e Silva, P. M. Engel, M. Trevisan, M. A. Idiart, Exploration method using harmonic functions, *Robotics and Autonomous Systems* 40 (1) (2002) 25–42.
- [2] I. Akduman, R. Kress, Electrostatic imaging via conformal mapping, *Inverse Problems* 18 (6) (2002) 1659.
- [3] R. Sharma, A. B. Farimani, J. Gomes, P. Eastman, V. Pande, Weakly-supervised deep learning of heat transport via physics informed loss, *arXiv preprint arXiv:1807.11374* (2018).
- [4] A. Galybin, J. Irša, On reconstruction of three-dimensional harmonic functions from discrete data, *Proceedings of the Royal Society A: Mathematical, Physical and Engineering Sciences* 466 (2119) (2010) 1935–1955.
- [5] M. Raissi, P. Perdikaris, G. E. Karniadakis, Physics-informed neural networks: A deep learning framework for solving forward and inverse problems involving nonlinear partial differential equations, *Journal of Computational physics* 378 (2019) 686–707.

- [6] L. Lu, R. Pestourie, W. Yao, Z. Wang, F. Verdugo, S. G. Johnson, Physics-informed neural networks with hard constraints for inverse design, *SIAM Journal on Scientific Computing* 43 (6) (2021) B1105–B1132.
- [7] G.-J. Both, S. Choudhury, P. Sens, R. Kusters, Deepmod: Deep learning for model discovery in noisy data, *Journal of Computational Physics* 428 (2021) 109985.
- [8] P. Shor, Algorithms for quantum computation: discrete logarithms and factoring, in: *Proceedings 35th Annual Symposium on Foundations of Computer Science*, 1994, pp. 124–134.
- [9] A. W. Harrow, A. Hassidim, S. Lloyd, Quantum algorithm for linear systems of equations, *Phys. Rev. Lett.* 103 (2009) 150502.
- [10] F. Arute, K. Arya, R. Babbush, D. Bacon, J. C. Bardin, R. Barends, R. Biswas, S. Boixo, F. G. Brandao, D. A. Buell, et al., Quantum supremacy using a programmable superconducting processor, *Nature* 574 (7779) (2019) 505–510.
- [11] H.-S. Zhong, H. Wang, Y.-H. Deng, M.-C. Chen, L.-C. Peng, Y.-H. Luo, J. Qin, D. Wu, X. Ding, Y. Hu, et al., Quantum computational advantage using photons, *Science* 370 (6523) (2020) 1460–1463.
- [12] M. Cerezo, A. Arrasmith, R. Babbush, S. C. Benjamin, S. Endo, K. Fujii, J. R. McClean, K. Mitarai, X. Yuan, L. Cincio, et al., Variational quantum algorithms, *Nature Reviews Physics* 3 (9) (2021) 625–644.
- [13] H. Kurt, S. Maxwell, W. Halbert, Multilayer feedforward networks are universal approximators, *Neural Networks* 2 (5) (1989) 359–366.
- [14] T. Goto, Q. H. Tran, K. Nakajima, Universal approximation property of quantum machine learning models in quantum-enhanced feature spaces, *Phys. Rev. Lett.* 127 (2021) 090506.
- [15] G. G. Guerreschi, M. Smelyanskiy, Practical optimization for hybrid quantum-classical algorithms, *arXiv preprint arXiv:1701.01450* (2017).
- [16] O. Kyriienko, V. E. Elfving, Generalized quantum circuit differentiation rules, *Physical Review A* 104 (5) (2021) 052417.
- [17] K. Mitarai, M. Negoro, M. Kitagawa, K. Fujii, Quantum circuit learning, *Phys. Rev. A* 98 (2018) 032309.
- [18] O. Kyriienko, A. E. Paine, V. E. Elfving, Solving nonlinear differential equations with differentiable quantum circuits, *Physical Review A* 103 (5) (2021) 052416.
- [19] A. E. Paine, V. E. Elfving, O. Kyriienko, Quantum quantile mechanics: Solving stochastic differential equations for generating time-series, *arXiv preprint arXiv:2108.03190* (2021).



- [20] N. Heim, A. Ghosh, O. Kyriienko, V. E. Elfving, Quantum model-discovery, arXiv preprint arXiv:2111.06376 (2021).
- [21] S. Varsamopoulos, E. Philip, H. W. T. van Vlijmen, S. Menon, A. Vos, N. Dyubankova, B. Torfs, A. Rowe, V. E. Elfving, Quantum extremal learning, arXiv preprint arXiv:2205.02807 (2022).
- [22] M. Schuld, N. Killoran, Quantum machine learning in feature hilbert spaces, *Physical review letters* 122 (4) (2019) 040504.
- [23] A. Abbas, D. Sutter, C. Zoufal, A. Lucchi, A. Figalli, S. Woerner, The power of quantum neural networks, *Nature Computational Science* 1 (6) (2021) 403–409.
- [24] H.-Y. Huang, M. Broughton, M. Mohseni, R. Babbush, S. Boixo, H. Neven, J. R. McClean, Power of data in quantum machine learning, *Nature Communications* 12 (1) (2021) 2631.
- [25] J. R. McClean, S. Boixo, V. N. Smelyanskiy, R. Babbush, H. Neven, Barren plateaus in quantum neural network training landscapes, *Nature communications* 9 (1) (2018) 1–6.
- [26] E. R. Anschuetz, B. T. Kiani, Beyond barren plateaus: Quantum variational algorithms are swamped with traps, arXiv preprint arXiv:2205.05786 (2022).
- [27] S. Hadfield, Z. Wang, B. O’gorman, E. G. Rieffel, D. Venturelli, R. Biswas, From the quantum approximate optimization algorithm to a quantum alternating operator ansatz, *Algorithms* 12 (2) (2019) 34.
- [28] K. Bharti, T. Haug, Iterative quantum-assisted eigensolver, *Physical Review A* 104 (5) (2021) L050401.
- [29] J. Kübler, S. Buchholz, B. Schölkopf, The inductive bias of quantum kernels, *Advances in Neural Information Processing Systems* 34 (2021).
- [30] Y. LeCun, L. Bottou, Y. Bengio, P. Haffner, Gradient-based learning applied to document recognition, *Proceedings of the IEEE* 86 (11) (1998) 2278–2324.
- [31] C. L. Giles, T. Maxwell, Learning, invariance, and generalization in high-order neural networks, *Applied optics* 26 (23) (1987) 4972–4978.
- [32] S. Greydanus, M. Dzamba, J. Yosinski, Hamiltonian neural networks, *Advances in Neural Information Processing Systems* 32 (2019).
- [33] P. Mernyei, K. Meichanetzidis, I. I. Ceylan, Equivariant quantum graph circuits, arXiv preprint arXiv:2112.05261 (2021).
- [34] M. Larocca, F. Sauvage, F. M. Sbahi, G. Verdon, P. J. Coles, M. Cerezo, Group-invariant quantum machine learning, arXiv preprint arXiv:2205.02261 (2022).

- [35] I. E. Lagaris, A. Likas, D. I. Fotiadis, Artificial neural networks for solving ordinary and partial differential equations, *IEEE transactions on neural networks* 9 (5) (1998) 987–1000.
- [36] A. Krishnapriyan, A. Gholami, S. Zhe, R. Kirby, M. W. Mahoney, Characterizing possible failure modes in physics-informed neural networks, *Advances in Neural Information Processing Systems* 34 (2021).
- [37] S. Wang, X. Yu, P. Perdikaris, When and why pinns fail to train: A neural tangent kernel perspective, *Journal of Computational Physics* 449 (2022) 110768.
- [38] A. D. Jagtap, G. E. Karniadakis, Extended physics-informed neural networks (xpinns): A generalized space-time domain decomposition based deep learning framework for nonlinear partial differential equations, *Communications in Computational Physics* 28 (5) (2020) 2002–2041.
- [39] S. Wang, Y. Teng, P. Perdikaris, Understanding and mitigating gradient flow pathologies in physics-informed neural networks, *SIAM Journal on Scientific Computing* 43 (5) (2021) A3055–A3081.
- [40] N. Sukumar, A. Srivastava, Exact imposition of boundary conditions with distance functions in physics-informed deep neural networks, *Computer Methods in Applied Mechanics and Engineering* 389 (2022) 114333.
- [41] G. E. Karniadakis, I. G. Kevrekidis, L. Lu, P. Perdikaris, S. Wang, L. Yang, Physics-informed machine learning, *Nature Reviews Physics* 3 (6) (2021) 422–440.
- [42] Z. Li, N. Kovachki, K. Azizzadenesheli, B. Liu, K. Bhattacharya, A. Stuart, A. Anandkumar, Fourier neural operator for parametric partial differential equations, *arXiv preprint arXiv:2010.08895* (2020).
- [43] L. Lu, P. Jin, G. E. Karniadakis, Deeponet: Learning nonlinear operators for identifying differential equations based on the universal approximation theorem of operators, *arXiv preprint arXiv:1910.03193* (2019).
- [44] M. D. Gunzburger, J. S. Peterson, J. N. Shadid, Reduced-order modeling of time-dependent pdes with multiple parameters in the boundary data, *Computer methods in applied mechanics and engineering* 196 (4-6) (2007) 1030–1047.
- [45] J. Hendriks, C. Jidling, A. Wills, T. Schön, Linearly constrained neural networks, *arXiv preprint arXiv:2002.01600* (2020).
- [46] J. Richter-Powell, Y. Lipman, R. T. Chen, Neural conservation laws: A divergence-free perspective, *arXiv preprint arXiv:2210.01741* (2022).
- [47] M. Cranmer, S. Greydanus, S. Hoyer, P. Battaglia, D. Spergel, S. Ho, Lagrangian neural networks, *arXiv preprint arXiv:2003.04630* (2020).

- [48] J. Lee, W. J. Huggins, M. Head-Gordon, K. B. Whaley, Generalized unitary coupled cluster wave functions for quantum computation, *Journal of chemical theory and computation* 15 (1) (2018) 311–324.
- [49] S. Hadfield, Z. Wang, E. G. Rieffel, B. O’Gorman, D. Venturelli, R. Biswas, Quantum approximate optimization with hard and soft constraints, in: *Proceedings of the Second International Workshop on Post Moores Era Supercomputing*, 2017, pp. 15–21.
- [50] T. Elsken, J. H. Metzen, F. Hutter, Neural architecture search: A survey, *The Journal of Machine Learning Research* 20 (1) (2019) 1997–2017.
- [51] H. R. Grimsley, S. E. Economou, E. Barnes, N. J. Mayhall, An adaptive variational algorithm for exact molecular simulations on a quantum computer, *Nature communications* 10 (1) (2019) 1–9.
- [52] M. Mohseni, A. T. Rezakhani, D. A. Lidar, Quantum-process tomography: Resource analysis of different strategies, *Physical Review A - Atomic, Molecular, and Optical Physics* 77 (3) (2008) 32322. [arXiv:0702131](#), [doi:10.1103/PhysRevA.77.032322](#).
- [53] C. E. Granade, C. Ferrie, N. Wiebe, D. G. Cory, Robust online Hamiltonian learning, *New Journal of Physics* 14 (10) (2012) 0–31. [arXiv:arXiv:1207.1655v1](#), [doi:10.1088/1367-2630/14/10/103013](#).
- [54] M. Greiter, V. Schnells, R. Thomale, Method to identify parent hamiltonians for trial states, *Physical Review B* 98 (8) (2018) 081113.
- [55] A. A. Gentile, B. Flynn, S. Knauer, N. Wiebe, S. Paesani, C. E. Granade, J. G. Rarity, R. Santagati, A. Laing, Learning models of quantum systems from experiments, *Nature Physics* 17 (7) (2021) 837–843.
- [56] J. Bak, D. J. Newman, D. J. Newman, *Complex analysis*, Vol. 8, Springer, 2010.
- [57] J. Bassey, L. Qian, X. Li, A survey of complex-valued neural networks, *arXiv preprint arXiv:2101.12249* (2021).
- [58] M. Schuld, Supervised quantum machine learning models are kernel methods (2021).
- [59] S. McArdle, T. Jones, S. Endo, Y. Li, S. C. Benjamin, X. Yuan, Variational ansatz-based quantum simulation of imaginary time evolution, *npj Quantum Information* 5 (1) (2019) 75.
- [60] X. Yuan, S. Endo, Q. Zhao, Y. Li, S. C. Benjamin, Theory of variational quantum simulation, *Quantum* 3 (2019) 191.

- [61] M. Motta, C. Sun, A. T. K. Tan, M. J. O'Rourke, E. Ye, A. J. Minnich, F. G. S. L. Brandão, G. K.-L. Chan, Determining eigenstates and thermal states on a quantum computer using quantum imaginary time evolution, *Nature Physics* 16 (2) (2020) 205–210.
- [62] Supplementary information.
- [63] V. Bergholm, J. Izaac, M. Schuld, C. Gogolin, M. S. Alam, S. Ahmed, J. M. Arrazola, C. Blank, A. Delgado, S. Jahangiri, et al., PennyLane: Automatic differentiation of hybrid quantum-classical computations, arXiv preprint arXiv:1811.04968 (2018).
- [64] A. Mari, T. R. Bromley, N. Killoran, Estimating the gradient and higher-order derivatives on quantum hardware, *Physical Review A* 103 (1) (2021) 012405.
- [65] J. D. Jackson, *Classical electrodynamics* (1999).
- [66] C. R. Harris, K. J. Millman, S. J. Van Der Walt, R. Gommers, P. Virtanen, D. Cournapeau, E. Wieser, J. Taylor, S. Berg, N. J. Smith, et al., Array programming with numpy, *Nature* 585 (7825) (2020) 357–362.
- [67] J. D. Hunter, Matplotlib: A 2d graphics environment, *Computing in science & engineering* 9 (03) (2007) 90–95.
- [68] M. Alnæs, J. Blechta, J. Hake, A. Johansson, B. Kehlet, A. Logg, C. Richardson, J. Ring, M. E. Rognes, G. N. Wells, The fenics project version 1.5, *Archive of Numerical Software* 3 (100) (2015).
- [69] A. Paszke, S. Gross, F. Massa, A. Lerer, J. Bradbury, G. Chanan, T. Killeen, Z. Lin, N. Gimelshein, L. Antiga, et al., Pytorch: An imperative style, high-performance deep learning library, *Advances in neural information processing systems* 32 (2019).
- [70] K. He, X. Zhang, S. Ren, J. Sun, Delving deep into rectifiers: Surpassing human-level performance on imagenet classification, in: *Proceedings of the IEEE international conference on computer vision*, 2015, pp. 1026–1034.
- [71] D. P. Kingma, J. Ba, Adam: A method for stochastic optimization, arXiv preprint arXiv:1412.6980 (2014).
- [72] X.-Z. Luo, J.-G. Liu, P. Zhang, L. Wang, Yao. jl: Extensible, efficient framework for quantum algorithm design, *Quantum* 4 (2020) 341.
- [73] D. C. Liu, J. Nocedal, On the limited memory bfgs method for large scale optimization, *Mathematical programming* 45 (1) (1989) 503–528.
- [74] E. Rimon, *Exact robot navigation using artificial potential functions*, Yale University, 1990.

- [75] C. I. Connolly, R. A. Grupen, The applications of harmonic functions to robotics, *Journal of robotic Systems* 10 (7) (1993) 931–946.
- [76] M. Kazemi, M. Mehrandezh, Robotic navigation using harmonic function-based probabilistic roadmaps, in: *IEEE International Conference on Robotics and Automation*, 2004. Proceedings. ICRA'04. 2004, Vol. 5, IEEE, 2004, pp. 4765–4770.
- [77] S. G. Loizou, The multi-agent navigation transformation: tuning-free multi-robot navigation., in: *Robotics: Science and Systems*, Vol. 6, 2014, pp. 1516–1523.
- [78] M. A. Nielsen, I. Chuang, *Quantum computation and quantum information* (2002).
- [79] J. B. Perot, C. J. Zusi, Differential forms for scientists and engineers, *Journal of Computational Physics* 257 (2014) 1373–1393.
- [80] S. H. Weintraub, *Differential forms: theory and practice*, Elsevier, 2014.